NASA Technical Memorandum 101584

FLUTTER SUPPRESSION CONTROL LAW SYNTHESIS FOR THE ACTIVE FLEXIBLE WING MODEL

Vivek Mukhopadhyay, Boyd Perry III, and Thomas E. Noll

MAY 1989

National Aeronautics and Space Administration

Langley Research Center
Hampton, Virginia 23665-5225

FLUTTER SUPPRESSION CONTROL LAW SYNTHESIS FOR THE ACTIVE FLEXIBLE WING MODEL

Vivek Mukhopadhyay
Planning Research Corporation
Hampton, Virginia 23666
United States

and

Boyd Perry III and Thomas E. Noll
NASA Langley Research Center
Hampton, Virginia 23665-5225
United States

ABSTRACT

The Active Flexible Wing Project is a collaborative effort between the NASA Langley Research Center and Rockwell International. The objectives are the validation of methodologies associated with mathematical modeling, flutter suppression control law development and digital implementation of the control system for application to flexible aircraft. A flutter suppression control law synthesis for this project is described here. The state-space mathematical model used for the synthesis included ten flexible modes, four control surface modes and rational function approximation of the doublet-lattice unsteady aerodynamics. The design steps involved developing the full-order optimal control laws, reducing the order of the control law, and optimizing the reduced-order control law in both the continuous and the discrete domains to minimize stochastic response. System robustness was improved using singular value constraints. An 8th order robust control law was designed to increase the symmetric flutter dynamic pressure by 100 per cent. Preliminary results are provided and experiences gained are discussed.

1. INTRODUCTION

An approach for developing a low-order, robust multi-input multi-output (MIMO) digital control law for application to flexible aircrafts is currently being evaluated as part of the NASA Langley Research Center (LaRC) and Rockwell International cooperative Active Flexible Wing (AFW) project.[1,2] The objective of these investigations is to obtain experimental data for validating the analysis, design and test methodologies associated with MIMO digital systems for flexible aircraft applications. The program spans approximately three years, and involves two test entries in the LaRC Transonic Dynamics Tunnel (TDT). One of the objectives of the first tunnel entry is to evaluate various active flutter suppression control laws obtained using advanced design methodology. To satisfy the goals of the program the FSS must be capable of suppressing both symmetric and antisymmetric flutter modes simultaneously.

A modern flexible aircraft with active control is typically modeled by a large order state-space system of equations in order to accurately represent the rigid and flexible body modes, unsteady aerodynamic forces, actuator dynamics, antialiasing filters and gust spectrum. The control law of this MIMO system is expected to satisfy a set of conflicting design requirements on the dynamic responses, actuator deflection and rate limitations. It should also be robust to the modeling uncertainty and should maintain certain stability margins over the test envelop, yet should be simple enough for implementation in a digital computer. Linear quadratic Gaussian (LQG) procedure is used for designing robust control laws for the linear multivariable system with modeling uncertainty. However, the resulting control law is of the same high-order as the design model and therefore, becomes difficult to implement for practical application. This paper describes development of a low-order, robust MIMO flutter suppression control law using LQG theory and constrained optimization technique.[3-6] Preliminary results are provided and experiences gained are discussed.

2. AFW MODEL DESCRIPTION

The AFW wind-tunnel model is an aeroelastically-scaled full-span model of an advanced tailless fighter configuration. It has a fuselage and low-aspect-ratio wings with a span of about nine feet. A photo of the sting-mounted model taken during a previous TDT entry is shown in Figure 1. A sketch of the model which shows the multiple control surfaces and accelerometer sensor placement is presented in Figure 2. As can be seen from the sketch, the aeroelastic model was modified to flutter within the TDT envelope by attaching ballast to the wing tips.

2.1 Structure

The structure of the model consisted of a "rigid" fuselage and "flexible" wings. The fuselage contained aluminum stringers and bulkheads but was not scaled for flexibility. The wing box contained an aluminum honeycomb core and tailored plies of graphite-epoxy. This wing design permitted desired amounts of bending and twist as a function of aerodynamic load to enhance manuverability. The model was statically and dynamically scaled to represent a full-scale airplane with a wing span of about 50 feet.

2.2 Control Surfaces and Sensors

The model has two leading-edge (LEI and LEO) and two trailing-edge (TEI and TEO) control surfaces on each wing panel (Figure 2). Each control surface had a chord of 25% of the local wing chord and a span of 28% of the wing semispan. Each control surface is driven by rotary-vane electrohydraulic actuators and each is capable of being used as an active-control surface. The actuators serve two functions: for constant inputs, to deflect control surfaces relative to the wing to minimize hinge moment at certain conditions; and for time-varying inputs, to deflect control surfaces in a manner dictated by the control law.

Twelve accelerometers mounted inside the model were used as sensors. Two of the accelerometers were located along the fuselage centerline. Five pairs of accelerometers were symmetrically located on each wing at the hingeline of the TEI, LEO and TEO control surfaces, at the wing tip and off-center on the fuselage. The model was also instrumented with strain-gauge bridges, a roll potentiometer, and a roll-rate gyro. The strain gauges were aligned to provide bending moment and torsion moment information.

3. MATHEMATICAL MODEL

The mathematical half-model used for the symmetric flutter evaluation included ten symmetric flexible modes and four control surfaces. The calculated flexible mode shapes, frequencies, and generalized masses were used. Table I contains the first 10 natural frequencies of the symmetric modes. All flexible modes were assumed to have a structural damping coefficient of 0.03.

3.1 Equations of Motion

The equations of motion were derived through a modal approach using Lagrange's equations, resulting in linearized small-perturbation matrix equations of the form

$$[M]\{\ddot{q}\}+[D]\{\dot{q}\}+[K]\{q\}+\frac{1}{2}\rho V^2[Q]\{q\}=\frac{1}{2}\rho V^2\{Q_g\}w_g \quad (1)$$

where M, D, and K are respectively the generalized mass, damping and stiffness matrices, Q and Q_g are the generalized aerodynamic force matrices due to vehicle motion and gust, q is the vector of generalized coordinates of structure and control modes, ρ is the fluid density, V is the velocity and w_g is the gust velocity. The aerodynamic force coefficients were determined by a doublet-lattice unsteady aerodynamics code[7].

3.2 Response Quantities

Response quantities included angular rate of roll and linear accelerations, shear forces, bending moments, and torsion moments at several locations on the wing. The rates and accelerations were obtained by weighting the generalized-coordinate rates and accelerations by modal slopes and deflections. The forces and moments were obtained by the mode displacement method of computing dynamic loads[8].

3.3 Analytical Model of Actuator Dynamics

The dynamics of the electrohydraulic actuators were modeled to best match frequency response test data. Third-order transfer functions were obtained analytically by employing parameter estimation techniques to match the magnitude and phase characteristics of the test data[1].

3.4 Control Surface Correction Factors

Because the wind-tunnel model was aeroelastically scaled, the aerodynamic effectiveness of each pair of surfaces varied significantly with dynamic pressure. The effectiveness was determined experimentally during a previous tunnel entry of this model. To more accurately model the change of control-surface effectiveness with increasing dynamic pressure, control surface correction factors were employed. These correction factors were derived by comparing analytical predictions of lift force and rolling moments with experimental data from the earlier TDT entry. The correction factors brought the analytically-corrected control-surface effectiveness into exact agreement with experimental data.

3.5 State-Space Equations

To obtain a set of constant coefficient differential equations, each element of the unsteady aerodynamic force matrices in equation (1) was approximated by a rational polynomial[9,10] in the Laplace variable, s. By equating derivatives to the powers of the Laplace variable, the equations of motion and response equations can be written in state-space form as shown in equations (2-4).

plant

$$dx_s/dt = F x_s + G_u u + G_w w \quad (2)$$

output

$$y = H x_s \quad (3)$$

design output

$$y_d = H_d x_s \quad (4)$$

control law

$$x_c = A x_c + B y$$
$$u = C x_c + D y \quad (5)$$

The plant equation (2), represents the linear equations of motion, due to a small perturbation from a steady state equilibrium condition. The control and gust input are u and w. The sensor output measurements y are modeled by equation (3). The design outputs which include control surface deflection and rate are modeled by equation (4). The equations (5) are state-space representation of a feedback control law driven by the output feedback y.

3.6 Open-loop Dynamic Pressure Root-locus

A plot of the open-loop dynamic pressure root-locus of the symmetric equations of motion at Mach 0.9 is shown in Figure 3. The arrows indicate the direction of increasing dynamic pressure. Only the flexible mode roots are shown. The sting mode is marked 1. The unstable interaction between the second and third flexible modes causes the open loop flutter to occur at a dynamic pressure of 225 pounds per square foot (psf) and at a frequency of 9.4 Hertz. The sixth and seventh flexible modes also seem to interact at a frequency near 29 Hertz.

4. MULTIVARIABLE CONTROL DESIGN PHILOSOPHY

The control law design considerations for a multivariable system are schematically described in Figure 4. A modern flexible aircraft with active control is typically modeled by a large order state-space system of equations in order to accurately represent the rigid and flexible body modes, unsteady aerodynamic forces, actuator dynamics, antialiasing filters and gust spectrum. The control law of this MIMO system is expected to satisfy a set of conflicting design requirements on the dynamic responses, actuator deflection and rate limitations. It should also be robust to the modeling uncertainty and should maintain certain stability margins over the test envelop, yet should be simple enough for implementation in a digital computer.

4.1 LQG Control Law Design and Order Reduction

The procedure for designing an initial low-order control law is schematically shown by the block diagram in Figure 5. Optimal control theory is used to design an initial linear quadratic Gaussian feedback control law of the form shown in equation (5). Since the full-order plant model is used for the design, the LQG control law is of the same large-order as the plant making it difficult to implement in a digital computer. Hence, the large-order controller must be reduced to a lower order without sacrificing the performance and stability robustness properties, substantially. A singular value analysis is used to determine the robustness of the full-order controller and to assist in determining the significant states to be retained in the reduced-order controller. The balanced truncation or residualization techniques are used for control law order reduction. The reduced-order control law is then checked for stability. If it is unstable, the designer can reselect the controller states to be retained in the reduction process or redesign the LQG controller with different sets of weighting and noise intensity matrices. Since the order reduction usually results in loss of stability robustness properties and increased RMS responses, it was necessary to optimize the reduced-order control law to improve its performance.

4.2 Optimization and Robustness Improvement

A constrained optimization technique[5,6] for improving the performance and stability robustness of the reduced-order control law is schematically shown in Figure 6. The parameters of the reduced-order stable control law which was determined using the procedure shown in Figure 5 are used as the design variables. This is represented by the first block in Figure 6. The synthesis procedure minimizes a standard LQG performance index, while attempting to satisfy a set of design constraints. The method of feasible direction is used to update the control law design variables. The design requirements, such as, control surface deflection and rate limits, maximum allowable RMS responses can be imposed as constraints. The constraints on the minimum singular value at the plant input and output are also used to improve the robustness properties. These conflicting requirements are imposed as constraints instead of lumping them into a performance index, since a stability margin improvement at the plant input is accompanied by a stability margin degradation at the plant output and an increase in response and control activity. The designer can choose the structure of the control law, the design variables and a set of inequality constraints. This enables optimization of a classical control law as well as an estimator based full- or reduced-order control law to meet specific design demands.

4.3 Design in Discrete Domain

For the discrete system, the complete state-space equations including the computational delay and antialiasing filters can be expressed as

plant

$$x_{k+1} = F x_k + G_u u_k + G_w w_k \quad (6)$$

output

$$y_k = H x_k \quad (7)$$

design output

$$y_{dk} = H_d x_k + E_d u_k \quad (8)$$

control law

$$z_{k+1} = A z_k + B y_k$$
$$u_k = C z_k + D y_k \quad (9)$$

These constant-coefficient finite-difference linear equations represent discrete-time equations of motion, due to a small perturbation from a steady state equilibrium condition for a flexible aircraft. They are derived from the corresponding continuous equations (2-5) using z transforms with zero-order hold or Tustin transforms followed by state-space realization. The subscript k represents the data at the *kth* sampling stage. The constrained optimization procedure[6] for a discrete system is very similar to that of the continuous system as shown in Figure 6. Since the implementation is done using a digital microprocessor, control law synthesis and stability robustness improvement and simulation in the discrete domain are necessary. Also, many of the design considerations unique to digital systems, such as the effects of discretization, sampling time, computational delay and antialiasing filters can be taken into account and compensated for during the design stage.

5. FLUTTER SUPPRESSION SYSTEM DESIGN

The objective of the flutter suppression system (FSS) design is to develop low-order robust discrete control laws which can be implemented on a real-time digital computer operating at 200 samples per second. The goal is to increase the open-loop symmetric flutter dynamic pressure by 100% percent without exceeding control-surface deflection and rate limits which are 5 degrees and 100 degrees per second respectively. The FSS system should be stable over the entire dynamic pressure range and have gain and phase margins of 0.5 to 2.0 and $\pm$ 45 degrees on each channel at a dynamic pressure 44% percent above the open-loop flutter condition.

A block diagram of a generic flutter suppression system (FSS) is shown in Figure 7. The model has eight control inputs and twelve accelerometer sensor outputs. The right and left wing sensor signals are split into symmetric and antisymmetric components since the FSS control laws were designed separately for the symmetric and antisymmetric motion. The right and left wing actuator feedback signals were constituted by blending the symmetric and antisymmetric control law output components.

5.1 Symmetric FSS Control Law Design

It was assumed that there was no coupling between the symmetric and antisymmetric modes. The FSS control laws were designed separately for the symmetric and antisymmetric motion. The block diagram used for the design of the symmetric FSS control law is shown in the Figure 8. The symmetric flutter suppression system used the wing LEO and TEO control surfaces as inputs and the accelerometer sensors located near the LEO and TEO actuator hinge lines as measurement outputs. The design model used for determining a preliminary symmetric FSS control law was a 26th order state-space math model at 300 psf. The model included elastic modes 1 through 4, 6th and 7th mode and one aerodynamic lag term[9] for each mode. Two third order actuator dynamics and a second-order Dryden gust spectrum model were included in the plant model. The control surface effectiveness corrections and inertial effects were not included for this preliminary design. Designs with first-order 25 Hertz antialiasing filters, first-order 100 Hertz and fourth order 100 Hertz Butterworth antialiasing filters were studied. The design results with the fourth-order 100 Hertz antialiasing filters are presented here. Second-order Pade approximation to represent 1 sampling interval (1/200 seconds) delay was also added at each sensor output to simulate computational delays. The antialiasing filters and sample time delay dynamics were added to the plant model because of the significant phase lag introduced by them.

5.2 LQG Design and Order Reduction

The initial symmetric FSS control law was designed in the continuous domain using the procedure shown in Figure 5. First a LQG design was studied with different weighting matrices on the design output, control input, and noise intensity matrices at the plant input and measurement input. The optimal regulator was designed with zero state weighting and unit control weighting matrices. The Kalman state estimator was designed with unit gust noise and 0.01 g (g is the gravitational acceleration) measurement noise. Since the state-space system contained non-minimal phase zeros, and many poorly controllable and observable states, the LQG/LTR technique was used with care to avoid unstable pole-zero cancellation. Only the stable LQG control laws were chosen for further evaluation. The full-order LQG control laws were analyzed for stability robustness properties using a singular value analysis. The most promising full-order LQG control laws were reduced in order by block diagonalization and then by 1) truncation retaining only the interacting flutter mode state estimates or by 2) balanced realization followed by modal residualization. In general, the second method required more effort and yielded higher order control laws. Using the first procedure, an 8th-order stable control law was obtained by retaining the 2nd, 3rd, 4th and 7th flexible mode state estimates. The reduced-order control law was then analyzed at the design condition for evaluating stability and robustness properties.

5.3 Optimization

The stable reduced-order control law was first optimized in the continuous domain without using constraints and then analyzed. The subsequent optimization process in the continuous domain included constraints on the minimum singular values for improving stability margins as outlined in Figure 6. The constrained optimization procedure was used to raise the minimum singular value of the return-difference matrix at the plant input and output to above 0.4. This guarantees MIMO gain and phase margins of at least 0.67 to 1.68 and $\pm$25 degrees, respectively. The singular value plot of the return-difference matrix at the plant input and output for the 8th-order optimized control law designed at 300 psf are shown in Figures 9a and 9b, respectively. Figure 9c shows the eigenvalue magnitude of the return difference matrix and is used to estimate the conservativeness of the multiloop system robustness properties predicted from the singular value plots. Since the eigenvalue lower bounds are nearly the same as the singular value lower bounds, the robustness predictions are not overly conservative. Figure 9d shows the complex determinant of the return difference matrix as a function of frequency and can be interpreted as a multiloop Nyquist plot. In this case, the origin is the critical point and the determinant should be well away from the origin to ensure overall stability robustness.

5.4 Performance Analysis

The closed loop system with the 8th-order control law was analyzed in the continuous and discrete domain. Figures 10a, 10b and 10c show typical transient responses of the LEO and TEO accelerometer sensors due to a step command input to the TEO control surface of the closed loop system for the a) reduced-order unoptimized control law, b) optimized control law, and c) optimized control law with one sampling interval delay in the discrete domain, respectively. The control surface deflection time history for the case (c) is shown in Figure 10d. Comparison of Figures 10a and 10b indicate improvement in the transient response after optimization. The discrete domain simulation in Figures 10c and 10d indicate that the transients take a longer time to damp out due to the effect of the one sample period time delay. In order to improve the performance, the

system should be reoptimized in the discrete domain. The symmetric RMS response due to a 1 foot per second RMS gust input was computed at 300 psf. The LEO and TEO control surface RMS deflections and rates were found to be 0.4 and 0.7 degrees and 27.0 and 50.0 degrees per second, respectively. With the LEO loop open, the system was stable and the gain and phase margins for this loop were 0 to 4.3 and $\pm 92^{o}$ degrees, respectively. With the TEO loop open, the system was unstable. The gain and phase margins of this loop were 0.57 to 2.7 and $\pm 35^{o}$ degrees, respectively.

The 8th order optimized control law was also tested for stability in the discrete domain at 150 psf, 200 psf, 250 psf and at 400 psf, using the 26th-order design model and at 200 and 300 psf using a full 68th order evaluation model (which included all the 10 flexible modes and 4 aero-lag terms for each mode). The system was found to be stable at all conditions except at 400 psf where the system was just unstable, indicating that the flutter dynamic pressure of the closed loop system was just below 400 psf.

6. CONCLUDING REMARKS

Control law synthesis and optimization procedures for obtaining a preliminary symmetric flutter suppression system for the AFW wind-tunnel model was described. An initial state-space mathematical model derived using doublet-lattice unsteady aerodynamics at Mach 0.9 was used for the design and analysis. The model also included actuator dynamics, a Dryden gust spectrum and antialiasing filters. The flutter suppression system used leading edge and trailing edge outboard actuators as control input and wing mounted accelerometer sensors located near the actuator hingeline as output. An optimal full-order control law was designed and then reduced to an 8th-order control law and finally optimized to minimize response. The multivariable system robustness at the plant input and output were evaluated using singular value properties and were improved using a constrained optimization procedure. Since the singular value based guaranteed stability margin estimates are usually conservative, classical gain and phase margins were also evaluated using the single-loop open test. These were close to the desired values but needed improvement. Based on the gust model used, the root-mean-square responses were well within the allowable limits. The 8th-order continuous and a corresponding discrete control law increased the symmetric flutter dynamic pressure to almost 400 psf.

7. REFERENCES

1. Noll, T.; Perry, B., III; Tiffany, S.; Cole, S.; Buttrill, C.; Adams, W., Jr.; Houck, J.; Srinathkumar, S.; Mukhopadhyay, V.; Pototzky, A.; Heeg, J.; McGraw, S.; Miller, G.; Ryan, R.; Brosnan, M.; Haverty, J.and Klepl, M.: Aeroservoelastic Wind Tunnel Investigations Using the Active Flexible Wing Model - Status and Recent Accomplishments., NASA TM-101570, AIAA Paper 89-1168, Presented at the 30th AIAA Structures, Structural Dynamics and Materials Conference in Mobile, Alabama, April 1989.

2. Noll, T.; Perry, B. III and Gilbert, M: Recent Activities within the Aeroservoelasticity Branch at the NASA Langley Research Center. Paper No. 89-056, presented at the European Forum on Aeroelasticity and Structural Dynamics 1989 held in Aachen, Federal Republic of Germany, April 1989.

3. Mukhopadhyay, V.: Active Control Law Synthesis for Flexible Aircraft. Paper presented at the 1988 ASME Annual Winter Meeting, DSC Vol. 10, Chicago, Illinois, Nov-Dec 1988.

4. Mukhopadhyay, V.; Pototzky, A. and Noll, T.: Control Law Synthesis and Optimization Software for Large Order Aeroservoelastic Systems. Presentation made at the Workshop on the Computational Aspects in the Control of Flexible Systems, Williamsburg, Virginia, July 1988.

5. Mukhopadhyay, V.: Digital Robust Control Law Synthesis Using Constrained Optimization. Presentation made at the Second NASA/Air Force Symposium on Recent Experiences in Multidisciplinary Analysis and Optimization, NASA/LaRC, September 1988.

6. Mukhopadhyay, V.: Digital Robust Control Law Synthesis Using Constrained Optimization. Journal of Guidance Control and Dynamics, Vol. 12, No. 2, March-April, 1989, pp. 175-181.

7. Geising, J. P.; Kalman, T. P., and Rodden, W. P.: Subsonic Unsteady Aerodynamics for General Configurations, Part I: Direct Application of the Nonplanar Doublet Lattice Method. AFFDL-TR-71-5, 1971.

8. Pototzky, A. S. and Perry, B. III: New and Existing Techniques for Dynamic Loads Analysis of Flexible Airplanes. Journal of Aircraft, Vol. 23, No. 4, April 1986, pp. 340-347.

9. Abel, I.: An Analytical Technique for Predicting the Characteristics of a Flexible Wing Equipped with an Active Flutter Suppression System and Comparison with Wind-tunnel Data. NASA TP - 1367, 1979.

10. Tiffany S. and Karpel, M.: Aeroservoelastic Modeling and Application Using Minimum State Approximation of Unsteady Aerodynamics., NASA TM-101574, AIAA Paper No. 89- 1188, Presented at the 30th AIAA Structures, Structural Dynamics and Materials Conference in Mobile, Alabama, April 1989.

Table 1. Analytical vibration frequencies of symmetric flexible modes

Mode	Frequency (Hertz)	Description
1	5.65	sting bending
2	6.21	first bending
3	12.0	first torsion
4	12.8	
5	22.3	
6	26.7	
7	35.7	
8	39.5	
9	41.1	
10	51.2	

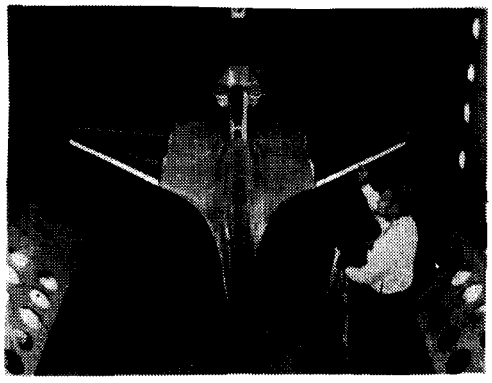

1. Active Flexible Wing (AFW) model in wind-tunnel.

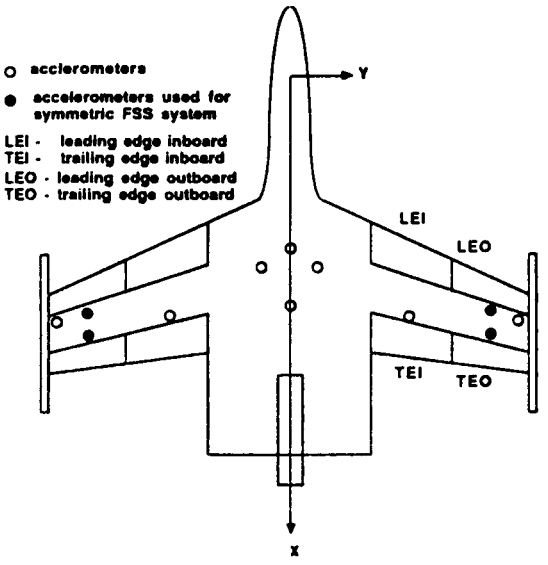

2. AFW control surface and accelerometer placement description.

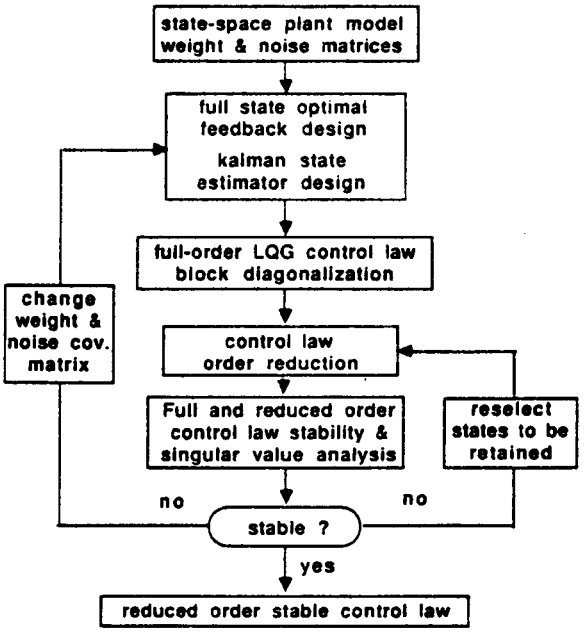

5. Control law order reduction procedure block diagram.

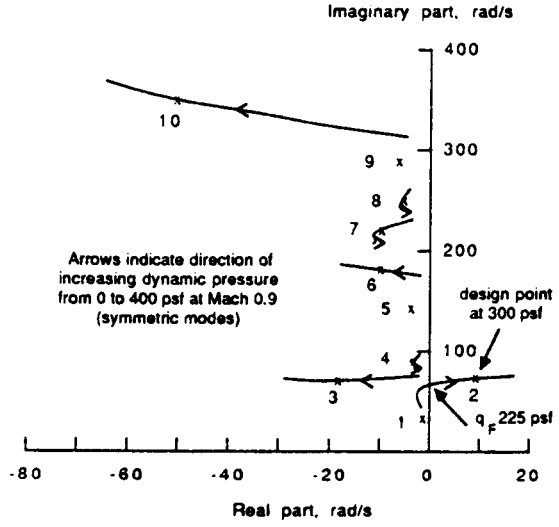

3. Open loop dynamic pressure root-locus of symmetric equations of motion at Mach 0.9.

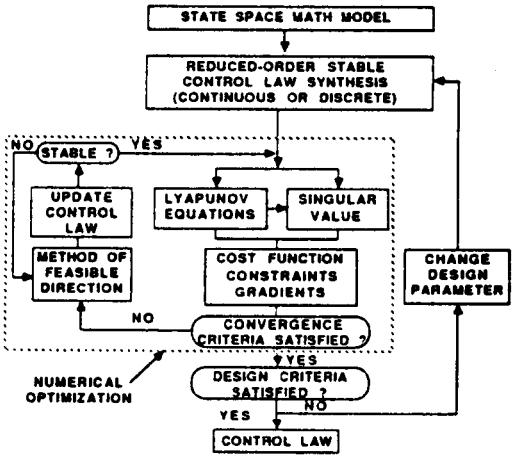

6. Control law optimization and robustness improvement procedure block diagram.

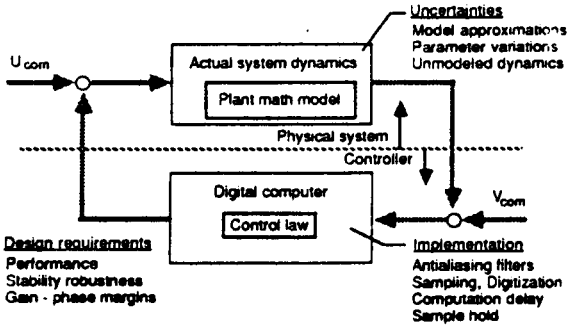

4. Design considerations for a multivariable control system

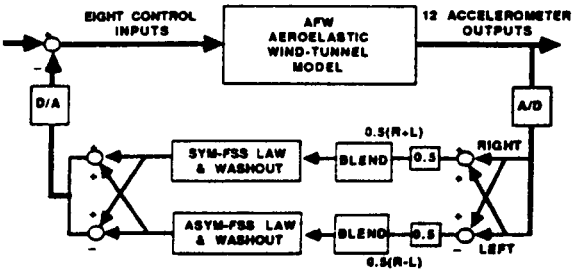

7. A generic flutter suppression system block diagram.

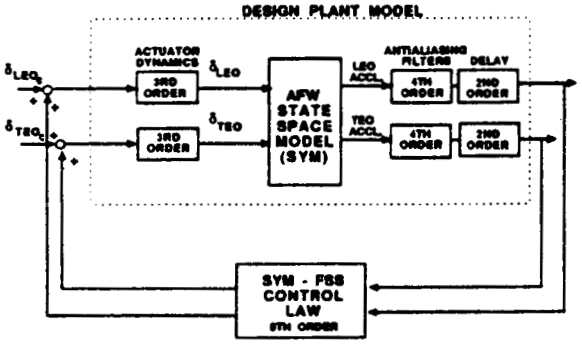

8. Symmetric flutter suppression system design block diagram.

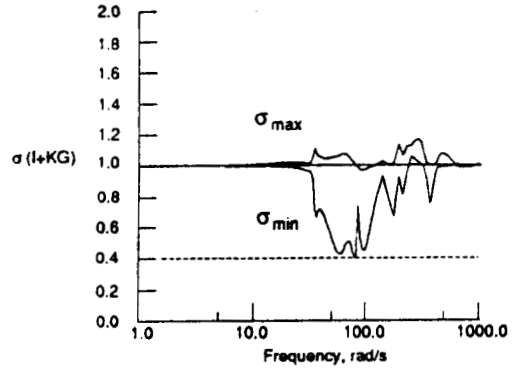

9a. Singular value plot of the return-difference matrix at plant input at the design dynamic pressure (300 psf).

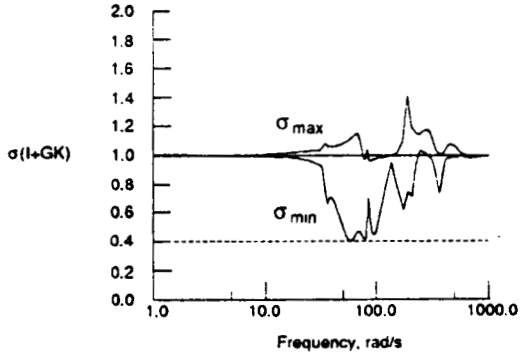

9b. Singular value plot of the return difference matrix at plant output at the design dynamic pressure (300 psf).

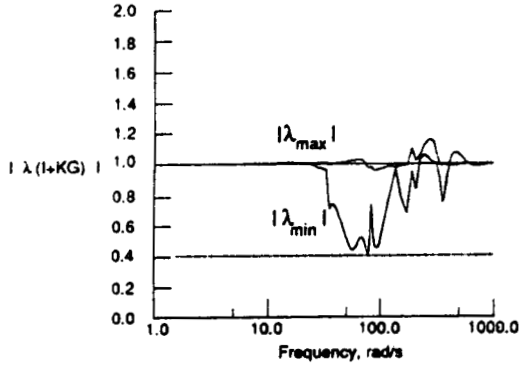

9c. Eigenvalue magnitude plot of the return-difference matrix at the design dynamic pressure (300 psf).

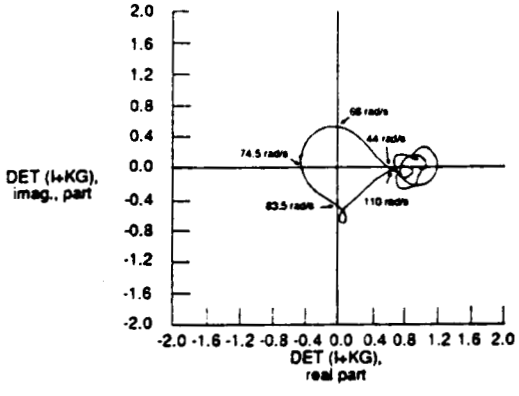

9d. Plot of the determinant of the return-difference matrix at the design dynamic pressure (300 psf).

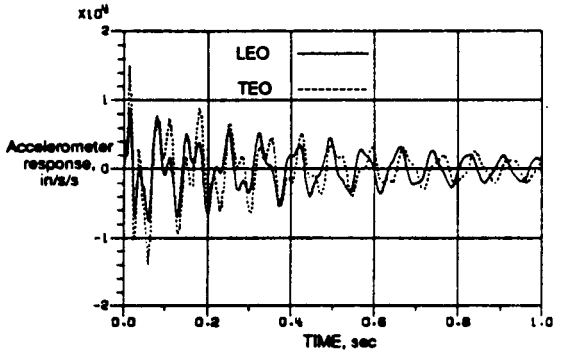

10a. Accelerometer transient response of closed-loop system at 300 psf due to unit step command at TEO actuator using reduced-order control law (continuous).

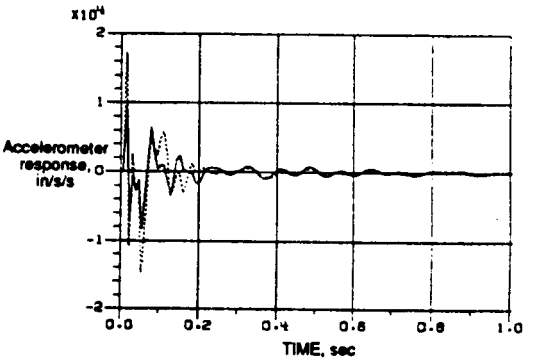

10b. Accelerometer transient response of closed-loop system at 300 psf due to unit step command at TEO actuator using optimized control law (continuous).

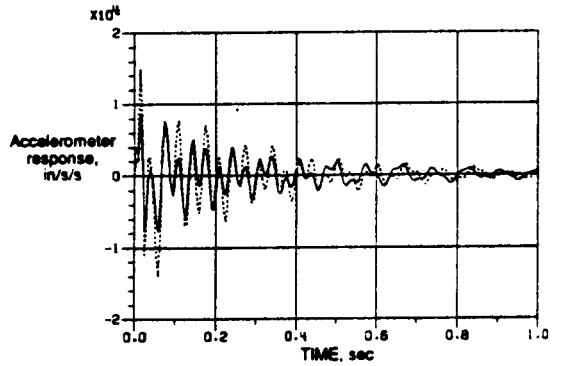

10c. Accelerometer transient response of closed-loop system at 300 psf due to unit step command at TEO actuator using optimized control law (discrete).

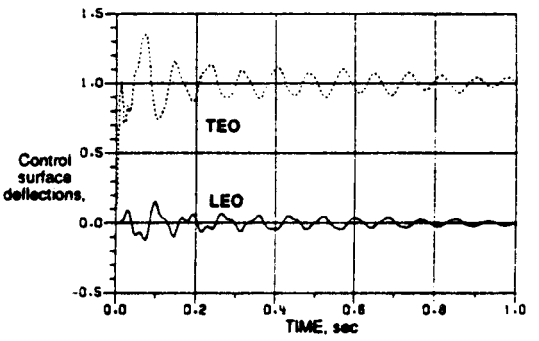

10d. Control surface deflections of closed-loop system at 300 psf due to unit step command at TEO actuator using optimized control law (discrete).

NASA
National Aeronautics and Space Administration

Report Documentation Page

1. Report No.	2. Government Accession No.	3. Recipient's Catalog No.
NASA TM-101584		

4. Title and Subtitle

Flutter Suppression Control Law Synthesis for the Active Flexible Wing Model

5. Report Date

May 1989

6. Performing Organization Code

7. Author(s)

Vivek Mukhopadhyay
Boyd Perry III
Thomas E. Noll

8. Performing Organization Report No.

10. Work Unit No.

505-63-21-04

9. Performing Organization Name and Address

NASA Langley Research Center
Hampton, VA 23665-5225

11. Contract or Grant No.

13. Type of Report and Period Covered

Technical Memorandum

12. Sponsoring Agency Name and Address

National Aeronautics and Space Administration
Washington, DC 20546-0001

14. Sponsoring Agency Code

15. Supplementary Notes

Presented at the European Forum on Aeroelasticity and Structural Dynamics, Aachen, Federal Republic of Germany, April 17-19, 1989.

16. Abstract

The Active Flexible Wing Project is a collaborative effort between the NASA Langley Research Center and Rockwell International. The objectives are the validation of methodologies associated with mathematical modeling, flutter suppression control law development and digital implementation of the control system for application to flexible aircraft. A flutter suppression control law synthesis for this project is described here. The state-space mathematical model used for the synthesis included ten flexible modes, four control surface modes and rational function approximation of the doublet-lattice unsteady aerodynamics. The design steps involved developing the full-order optimal control laws, reducing the order of the control law, and optimizing the reduced-order control law in both the continuous and the discrete domains to minimize stochastic response. System robustness was improved using singular value constraints. An 8th order robust control law was designed to increase the symmetric flutter dynamic pressure by 100 percent. Preliminary results are provided and experiences gained are discussed.

17. Key Words (Suggested by Author(s))

Flutter Suppression
Optimal Control Theory
Constrained Optimization
Robust Controller
LQG/LTR
Singular Value
Active Control
Low-Order Control Law
Aeroservoelasticity

18. Distribution Statement

Unclassified - Unlimited

Subject Category - 08

19. Security Classif. (of this report)	20. Security Classif. (of this page)	21. No. of pages	22. Price
Unclassified	Unclassified	8	A02